$c.1$

MOTION OF LIQUID-VAPOR INTERFACE IN RESPONSE TO IMPOSED ACCELERATION

by *William J. Masica* and *Donald A. Petrash*

Lewis Research Center
Cleveland, Ohio

MOTION OF LIQUID-VAPOR INTERFACE IN

RESPONSE TO IMPOSED ACCELERATION

By William J. Masica and Donald A. Petrash

Lewis Research Center
Cleveland, Ohio

NATIONAL AERONAUTICS AND SPACE ADMINISTRATION

MOTION OF LIQUID-VAPOR INTERFACE IN

RESPONSE TO IMPOSED ACCELERATION

by William J. Masica and Donald A. Petrash

Lewis Research Center

SUMMARY

As a part of the general study of the behavior of liquid propellants stored in space-vehicle tanks while exposed to weightlessness, an experimental investigation was conducted to determine the motion of the liquid-vapor interface in a cylindrical container in response to a constant translational acceleration. The imposed acceleration was applied parallel to the longitudinal axis of the cylinder and was directed positively from the vapor to the liquid phase separated by an initially highly curved interface. The results indicated that the liquid-vapor interface profile assumes the form predicted by the inviscid potential theory of G. I. Taylor. The rate at which the vapor phase penetrates the liquid phase (the ullage velocity) was empirically correlated as a function of known system parameters for Bond numbers greater than 1 and fluids possessing low viscosities. The leading edge of the liquid-vapor interface was found to accelerate over distances comparable to fineness ratios of 2; the magnitude of acceleration is a known function of ullage velocity.

INTRODUCTION

The advent of the more complex space missions has accentuated the necessity of obtaining optimum solutions to the problems associated with liquid-vapor systems in a weightless, or zero-gravity, environment. In particular the use of increasingly sophisticated space vehicles with liquid-propellant propulsion systems demands efficient tank venting and reliable engine restart capabilities following periods of weightlessness encountered in coasting flight. The theoretical studies of the parameters defining the static configuration and position of the liquid-vapor interface for conditions under which no external accelerations disturb the system after entering weightlessness is extensive and has been experimentally verified (A summary, for example, is given in ref. 1.). Realistic space vehicles, however, will be subjected to a variety of disturbances resulting from shutdown transients, orientation maneuvers, atmospheric drag in low Earth orbits, etc. In general, these disturbances will occur at all angles to the vehicle thrust axis and will tend to disrupt the established liquid-vapor interface and cause vapor to move in the direction of the acceleration.

The formulation of the dimensionless Bond number grouping, consisting essentially of the ratio of acceleration to capillary forces, has led to the successful correlation of the magnitude of acceleration required to disrupt the

equilibrium liquid-vapor interface (refs. 2 to 4). The critical Bond number delineating the stable and unstable regions in cylinders was shown to be independent of the liquid properties, the radial dimension, and the applied acceleration field and has been verified to be 0.84 for solid-liquid-vapor systems possessing 0° contact angles (ref. 5). However, the dynamic behavior of the liquid-vapor interface under the influence of random acceleration perturbations resulting in Bond numbers greater than critical is still largely unknown. As is easily verified by the most cursory of literature searches (e.g., bibliography in ref. 6), considerable attention has been focused on the control and stability problems associated with propellant sloshing during the powered phase of the flight but very little on the gross motion of the propellant under conditions of zero gravity or low-gravity-induced environments. While the former problems are indeed significant, the latter aspects of propellant behavior have recently generated considerable interest primarily because of the proposed use of auxiliary thrustors designed to position or reorient the liquid-vapor interface by inducing a low-body-force environment sufficiently prior to either main engine restart or venting operations. The dynamic behavior of the liquid-vapor interface during this reorientation or collection mode is of immediate interest. The initial conditions of the interface prior to the application of the imposed acceleration will determine the mode of liquid flow. Just as the stability characteristics of a plane interface are quite different from those of a spheroidal interface, the unstable mode in each instance will be similarly affected. In this investigation the initial system conditions resulted in a highly curved interface (i.e., low initial Bond number loading) prior to the application of the imposed acceleration.

The mode of liquid flow following the disruption of the interface under the action of low-level-acceleration induced body forces has been noted in a pilot experimental program (ref. 7), and a correlation of the significant parameters governing the velocity of the interface based on scaled experiments conducted at normal gravity conditions has been established (ref. 2). No other investigations directed immediately toward the collection of propellants are apparent; however, a large portion of theoretical and experimental work dealing with fluid dynamics exists that is applicable to the motion of the interface in response to low accelerations. The inviscid potential theory of Taylor describing the draining of liquids from closed, vertical circular tubes (ref. 8), for example, has formed the basis for the previously mentioned investigations. Other papers (refs. 9 to 11) have extended the theory to viscous systems and have provided sufficient background for explicit correlation of low-acceleration flow phenomenon in simple geometries.

The purpose of this report is to present the results of an experimental investigation conducted at the NASA Lewis Research Center of the motion of the liquid-vapor interface contained in a cylinder in response to an imposed acceleration. An extensive program was first conducted under normal-gravity conditions (i.e., 1 g) to extend the existing correlation of ascending bubble velocity in closed vertical cylinders. The empirical relation obtained, the resultant profile following the disruption of the interface, and an estimate of the instantaneous leading edge velocity were then verified as functions of low acceleration (< 1 g) and the pertinent system parameters. The latter investigation was conducted in a 2.3-second zero-gravity drop-tower facility to allow the liquid-vapor interface to approach its zero-gravity equilibrium configuration and to provide a proper environment for the induced low-acceleration field.

SYMBOLS

a	system acceleration, cm/sec^2
a_L	interface leading-edge acceleration, cm/sec^2
Bo	Bond number, $Bo = aR^2/\beta$
Fr	Froude number, $Fr = V_o/(aR)^{1/2}$
R	cylinder radius, cm
Re	Reynolds number
V_o	vapor penetration rate, or ullage velocity, cm/sec
x_L	interface leading-edge displacement, cm
x_o	vapor, or ullage, displacement, cm
β	specific surface tension, σ/ρ, cm^3/sec^2
η	liquid viscosity, cP
ρ	liquid density, gm/cm^3
σ	surface tension, dynes/cm

RESULTS AND DISCUSSION

Previous Investigations

The motion of long or infinite bubbles in closed, vertical cylindrical containers (fig. 1, p. 4) has attracted the interest of many investigators. A summary of their work appears in reference 9. Graphic descriptions of the rate at which the vapor phase penetrates the liquid phase, or the ascending bubble velocity, as a function of cylinder diameter for a particular liquid are presented in references 10 and 12. Although no explicit expression for the bubble velocity was obtained, three distinct regions characteristic to long bubble motion were apparent from these studies. In terms of the Bond number

$$Bo = \frac{aR^2}{\beta} \qquad (1)$$

where the density of the vapor phase has been neglected, the following three regions may be delineated:

  (1) 0.84 < Bo < 1.05

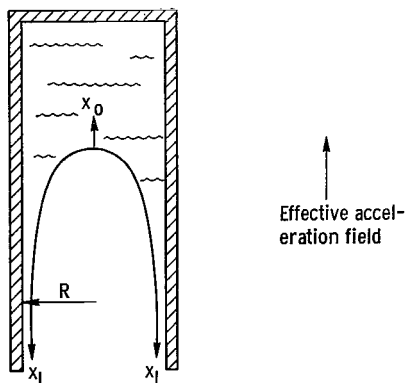 (2) 1.05 < Bo < 10

  (3) Bo > 10

3

Figure 1. - Interface profile under imposed acceleration directed perpendicular from vapor to liquid phase (where x_0 is vapor penetration displacement and x_L is leading-edge displacement).

For Bond numbers less than 0.84, the bubble remains stationary, in accordance with the known value of the critical Bond number. In the first region (0.84 < Bo < 1.05) Bretherton obtained from lubrication theory the following equation for the velocity of the bubble (ref. 11):

$$1.25\left(\frac{\eta V_0}{\sigma}\right)^{2/9} + 2.24\left(\frac{\eta V_0}{\sigma}\right)^{1/3} = Bo - 0.842 \qquad (2)$$

where η and σ are the viscosity and the surface tension of the liquid, respectively. The expression has not, however, been experimentally verified. The third region (Bo > 10), indicating in accordance with equation (1) that capillarity is becoming negligible, has been described in terms of Taylor's inviscid potential theory (ref. 8), where it was shown that

$$V_0 = 0.464 \ (aR)^{1/2} \qquad (3)$$

Taylor did verify this relation to his own satisfaction, although the experiments were abbreviated and indicated differing numerical constants. The region of intermediate Bond numbers has not been described by analytic theory, but the investigations previously reported have indicated a strong dependence of bubble velocity on surface tension (or equivalently, Bond number).

An empirical correlation employing Taylor's theory and the apparent dependence on the Bond number has been suggested by reference 2:

$$V_0 = 0.51(aR)^{1/2}\left[1 - \frac{1.12}{Bo}\right]\left[f(Re)\right], \ Bo > 1.75 \qquad (4)$$

where f(Re) is an empirically obtained correction factor based on the Reynolds number that approaches 1 as Re approaches 200. It is noted that equation (4) reduces to equation (3) for high Bond numbers differing only in the constant. Since the Reynolds number is itself a function of the unknown velocity, equation (4) does not, however, easily allow for the calculation of V_0 in the intermediate Bond number region.

Motion of Liquid-Vapor Interface in Normal-Gravity Field

Vapor penetration rate. - In order to establish firmly the correlation of the ascending bubble velocity, an experimental program was conducted at normal-gravity conditions through a carefully documented region of Bond numbers ranging from 3.49 to 1870. The cylinders producing Bond numbers less than 34 had precision bore diameters uniform to ±0.01 millimeter to establish the transition region to Taylor flow. To eliminate any end effects, the fineness ratios (length to diameter) of all the cylinders were greater than 10 to 1. The chemically pure liquids used in this study were restricted to those possessing low
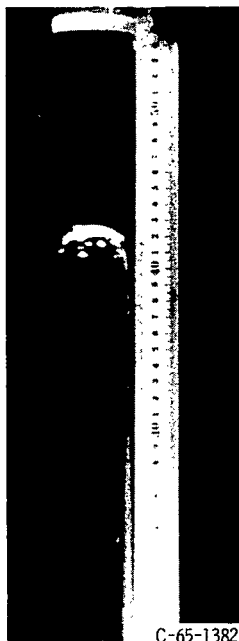
viscosities (of the order of 1 cP) and $0°$ contact angles on the borosilicate glass tubing employed in the study. To ensure perfect wetting, the cylinders were carefully cleaned by the same procedure as used for the low-acceleration investigation (see appendix). After alining the tubing to within $1°$ of true vertical, the cylinders were filled and drained similar to the manner reported in references 8 and 9. All data were taken by high-speed photographic techniques; a typical frame appears in figure 2.

The results of the normal-gravity investigation are shown in figure 3, where the Froude number, defined as the ratio of the bubble velocity to the square root of the acceleration times the radius of the cylinder, is plotted as a function of the Bond number. The equation

$$V_O = 0.48(aR)^{1/2}\left[1 - \left(\frac{0.84}{Bo}\right)^{Bo/4.7}\right] \tag{5}$$

was obtained by a curve fitted to these data employing the two limiting boundary conditions

$$V_O = 0 \qquad \text{for} \quad Bo \leq 0.84$$

$$V_O = K(aR)^{1/2} \qquad \text{for} \quad Bo \gg 10$$

Figure 2. - 1-g Bubble motion. Tube inside diameter, 4.67 centimeters; Bond number, 455; vapor penetration rate, 22.9 centimeters per second.

obtained from the author's previous studies and Taylor's potential theory. The relation describes the data in the Bond number region 3.49 to 1870 to within 5 percent. In order to further substantiate equation (5) and to determine the lower limit of its validity with respect to Bond number, the data in references 8 to 10 were plotted in figure 4 together with this empirical equation. The agreement of the equation with the published experimental data is remarkable and is seen even to include Bond numbers approaching 1. The validity of
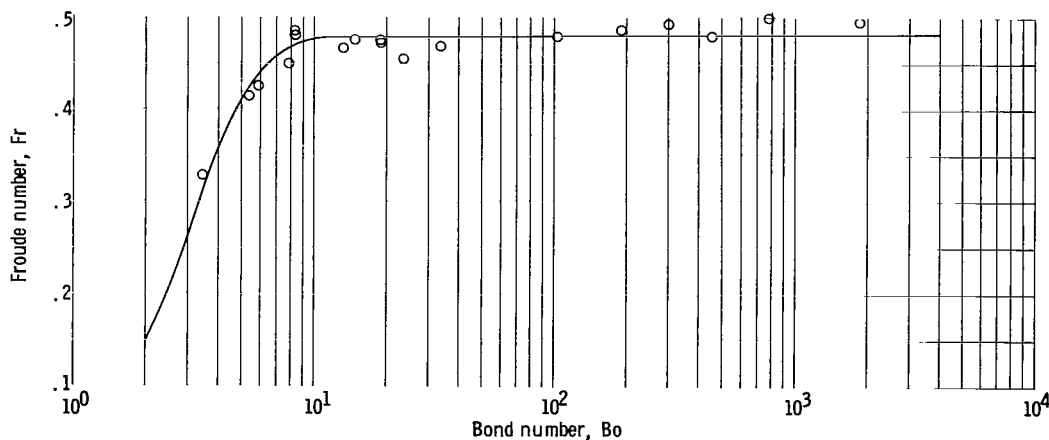
Figure 3. - Results of normal-gravity investigation. Liquid viscosity, 0.7 to 1.2 centipoise.
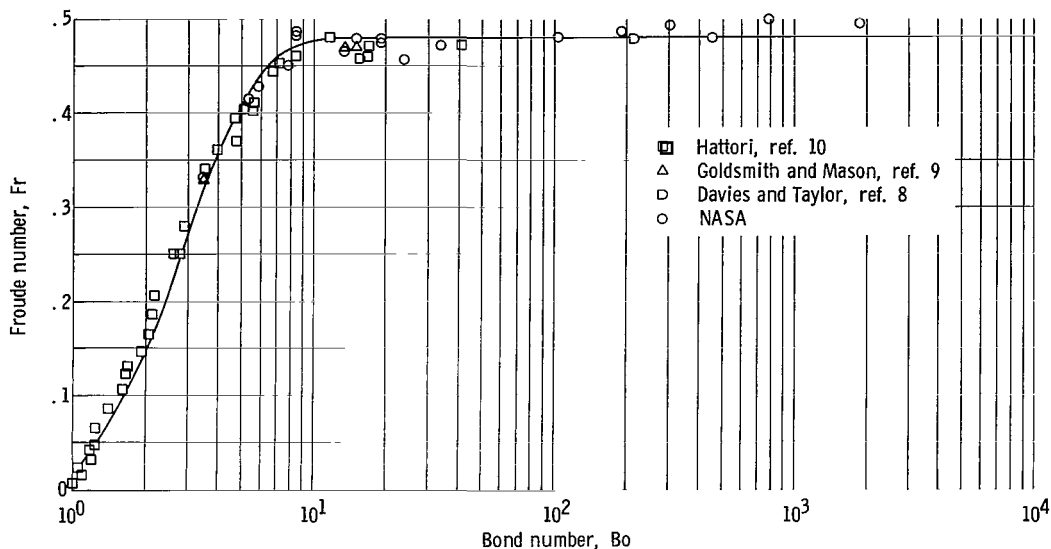
5

Figure 4. - Correlation of published data. System acceleration, 980 centimeters per second squared; liquid viscosity, 0.25 to 5.6 centipoise.

equation (5) for Bond numbers greater than 1 and low-viscosity fluids is firmly established. A summary of all the pertinent parameters involved in the normal-gravity investigation is contained in table I. It is noted that the Taylor region begins at a Bond number of 12, so that

$$V_O = 0.48(aR)^{1/2} \qquad \text{for} \quad Bo > 12 \qquad (6)$$

The constant differs from those in equations (3) and (4) by several percent.

Leading-edge displacement. - The method of initiating the bubble motion in normal gravity does not permit the motion of the leading edge of the interface to be examined. It is expected from Taylor's theory of inertia flow that the leading edge should accelerate freely with the magnitude given by the normal gravitational acceleration. The basic correlation of the rate of penetration of the vapor phase (eq. (6)) with Taylor's theory (eq. (3)) for Bond numbers greater than 12 effectively substantiates this assumption regarding the motion of the leading edge, at least under normal gravity conditions. In low-acceleration environments, however, the assumption of inertia flow may not be entirely valid, as the viscous forces at the wall might very well cause the leading edge to reach a terminal velocity rapidly. In order to establish the motion of the leading edge of the interface and to verify that the rate of penetration of the vapor phase as a function of acceleration is correctly given by equation (5), the experimental investigation was continued in low-acceleration environments.

Motion of Liquid-Vapor Interface in Low-Acceleration Field

Experimental limitations. - The apparatus and procedure used to obtain low-acceleration fields (less than 1 g) are given in the appendix. The results of this low-acceleration investigation may be first examined in terms of a representative run in which two cylinders, differing in radii but containing identi-

6

TABLE I. - SUMMARY OF PARAMETERS

Liquid	Cylinder radius, R, cm	Surface tension, σ, dynes/cm	Density, ρ, g/cm³	Liquid viscosity, η, cP	Vapor penetration rate, V_o, cm/sec	Froude number, Fr	Bond number, Bo	Specific surface tension, β, cm³/sec²
NASA[a]								
Trichlorotrifluoroethane	0.476	18.6	1.579	0.7	10.27	0.475	18.9	11.78
	1.11	↓	↓	↓	15.8	.479	103.0	↓
	2.34				22.9	.479	455.0	
	4.77				33.8	.494	1870.0	
	.635				11.7	.47	33.5	
	.476				10.2	.472	18.9	
	.317				8.5	.481	8.38	
	.317				8.55	.484	8.38	
Anhydrous ethanol	2.34	22.3	0.789	1.2	23.3	0.487	190.0	28.25
	4.77	↓	↓	↓	34.2	.5	780.0	↓
	.635				11.9	.477	14.9	
	.476				9.7	.45	7.86	
	.317				5.8	.33	3.49	
Distilled water[b]	4.77	72.75	1.0	1.0	33.7	0.493	303.0	72.75
	.635	72.75	1.0	1.0	10.4	.417	5.43	72.75
Carbon tetrachloride	0.317	26.8	1.595	0.97	7.55	0.427	5.86	16.79
	.635	26.8	1.595	.97	11.35	.455	23.4	16.79
	.476	26.8	1.595	.97	10.1	.467	13.2	16.79
Taylor								
Water	0.615	72.75	1.0	1.0	[c]9.94	0.405	5.09	72.7
	1.08	72.75	1.0	1.0	[c]14.88	.458	15.7	72.7
	3.97	72.75	1.0	1.0	[c]29.83	.478	212.0	72.7
Goldsmith and Mason								
Silicone oils	0.500	18.7	[d]1.15	2.5	[e]10.39	0.47	15.7	16.26
	.500	19.5	[d]1.08	5.6	[e]10.39	.47	13.5	18.06
Water	0.500	71.6	[d]1.02	1.0	[e]7.31	0.33	3.49	70.2
Hattori[f,g]								
Water	0.64	----	----	1.06	10.0	0.4	5.49	73.06 at 17.75° C
	.71	----	----	1.06	11.67	.442	6.76	73.06 at 17.75° C
	1.11	----	----	1.06	15.16	.46	16.5	73.06 at 17.75° C
	0.405	----	----	1.20	4.12	0.205	2.17	73.91 at 13° C
	.465	----	----		6.05	.28	2.87	↓
	.525	----	----		7.76	.342	3.66	
	.55	----	----		8.41	.362	4.01	
	.35	----	----		1.98	.107	1.62	
	.30	----	----		.532	.031	1.19	
	.29	----	----		.27	.016	1.11	
	.275	----	----	↓	.121	.007	1.00	
	0.595	----	----	1.11	9.54	0.395	4.72	73.5 at 15.8° C
	.38	----	----	1.11	2.82	.146	1.93	73.5 at 15.8° C
	.30	----	----	1.11	.715	.042	1.20	73.5 at 15.8° C
	0.26	----	----	1.24	~0.002	~0.00013	0.89	74.12 at 11.7° C
	.30	----	----	1.24	.633	.037	1.19	74.12 at 11.7° C
	.28	----	----	1.24	.142	.009	1.04	74.12 at 11.7° C
	0.35	----	----	0.79	2.26	0.122	1.68	71.36 at 30.7° C
	.30	----	----	.79	.785	.046	1.24	71.36 at 30.7° C
	.275	----	----	.79	.299	.018	1.04	71.36 at 30.7° C
Anhydrous ethanol	1.11	----	----	1.28	15.55	0.471	41.5	29.1 at 16.9° C
	.71	----	----	1.28	12.38	.471	17.0	29.1 at 16.9° C
	.64	----	----	1.28	11.63	.467	13.8	29.1 at 16.9° C
	0.465	----	----	1.39	9.64	0.45	7.21	29.39 at 12.6° C
	.405	----	----		8.00	.402	5.47	↓
	.38	----	----		7.10	.37	4.82	
	.29	----	----		4.15	.25	2.81	
	.225	----	----		1.14	.077	1.69	
	0.195	----	----	1.44	0.905	0.065	1.26	29.57 at 10.75° C
	.18	----	----	1.44	.079	.006	1.07	29.57 at 10.75° C
	.225	----	----	1.44	1.96	.13	1.68	29.57 at 10.75° C
	.26	----	----	1.41	2.97	.186	2.25	29.43 at 12.1° C
Diethyl ether	0.55	----	----	~0.25	11.2	0.482	11.72	25.3 at 10° C
	.465	----	----		9.81	.46	8.38	↓
	.38	----	----		7.78	.41	5.6	
	.3	----	----		5.87	.34	3.48	
	.26	----	----		3.95	.25	2.62	
	.19	----	----		1.17	.086	1.4	
	.165	----	----	↓	.292	.023	1.05	

[a]NASA data, parameters at 20° C.
[b]Maximum ionic impurity concentration, 1 ppm (with reference to sodium chloride).
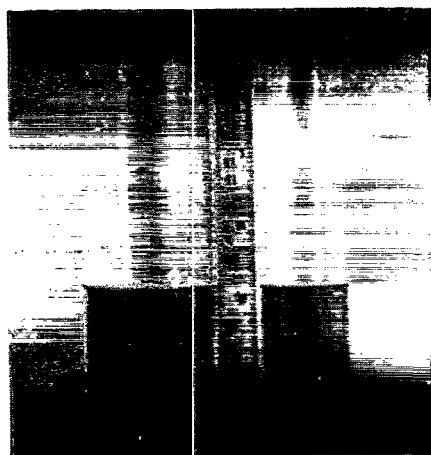[c]Average values.
[d]Obtained from given Reynolds no.
[e]Calculated from given Froude no.
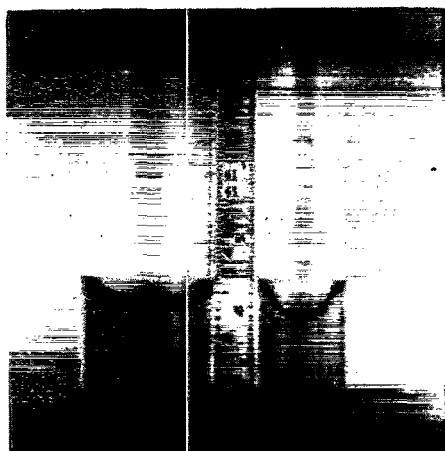[f]Viscosities obtained from handbook values at given liquid temperature.
[g]β calculated from ideal variation with temperature for given liquids

(a) 1-g Configuration: 0 second.

(c) 0-g Formation period; 0.42 second.

(b) 0-g Formation period; 0.25 second.

(d) Initiation of applied acceleration; 0.76 second.

Figure 5. – Interface velocity profile during representative data run.

cal liquids, are subjected to a common imposed acceleration. Photographs il-
lustrating the behavior of the liquid-vapor interface during the entire portion
of this representative test run are shown in figure 5; the liquid is trichloro-
trifluoroethane, the imposed acceleration is 36.3 centimeters per second
squared, and the radii are 1.27 and 2.03 centimeters for the right and left
cylinders, respectively. The resultant Bond numbers are 5.0 and 12.7. The
displacements of the leading edges of the interface x_L and the vapor or ullage
penetrations into the liquid x_0 are given in figure 6 as functions of time.
As may be seen from this figure, the 0.76 second allowed for the formation of
the zero-gravity equilibrium configuration was not sufficient to ensure com-
pletely quiescent conditions prior to the initiation of the imposed accelera-
tion; that is, both the leading edge and the vapor penetration have finite
velocities at thrust application. As such, the formation period during each
test run represents an initial perturbation to the desired regular mode of
liquid flow, and a transition region occurs prior to steady-state regular flow.
The net result of this perturbation is to reduce the acquisition of steady-
state flow data and to compound the probable error of measurement. The time
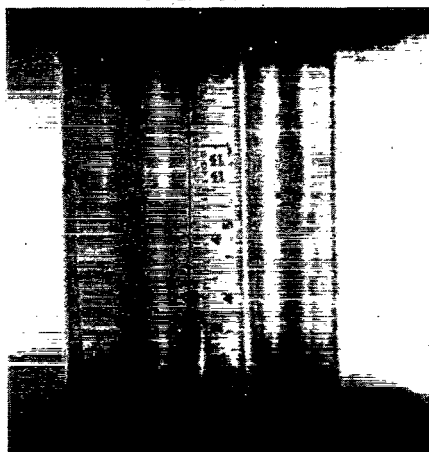
8

Applied acceleration
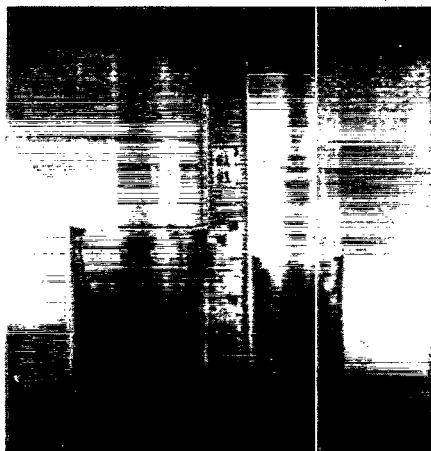
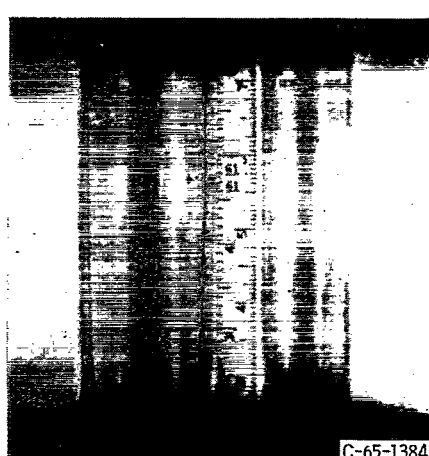(e) 0.94 Second.

Applied acceleration
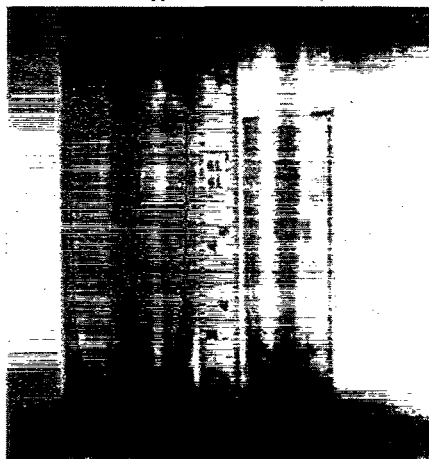
(h) 1.51 Seconds.
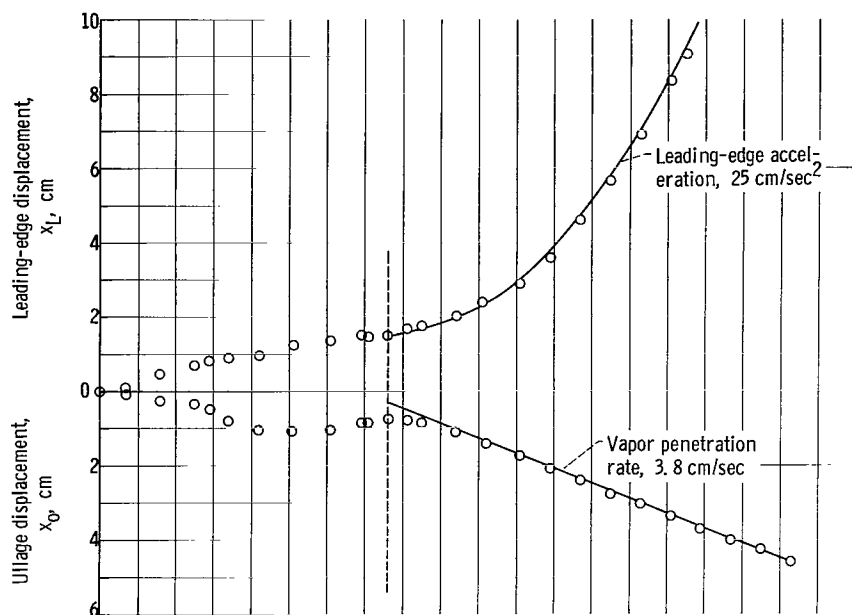

(f) 1.19 Seconds.

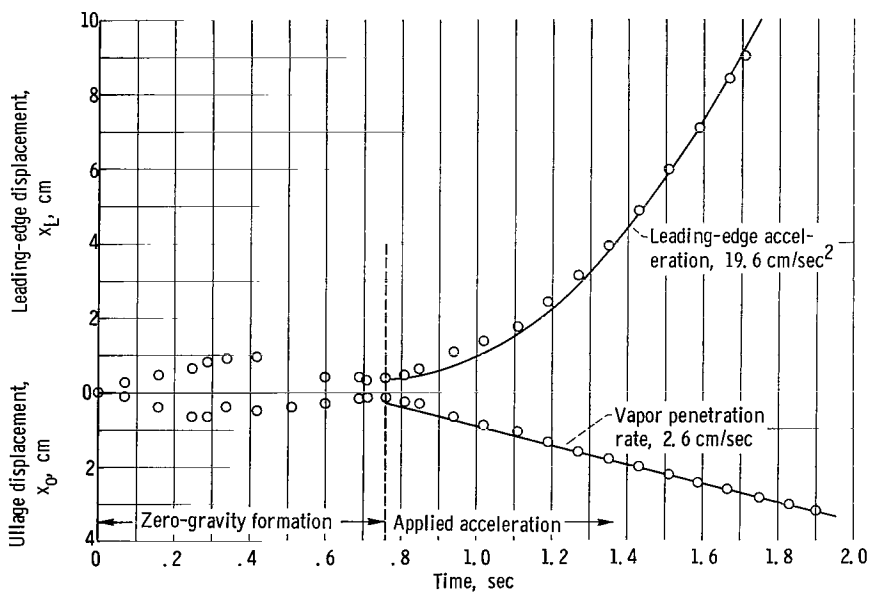(i) 1.71 Seconds.

(g) 1.35 Seconds.

C-65-1384

(j) 1.83 Seconds.

Figure 5. - Concluded.

9

(a) Cylinder radius, 2.03 centimeters.

(b) Cylinder radius, 1.27 centimeters.

Figure 6. - Interface displacement characteristics during representative data run.

TABLE II. - SUMMARY OF PARAMETERS IN LOW-ACCELERATION ENVIRONMENT INVESTIGATION

Liquid	Specific surface tension, β, cm^3/sec^2	Cylinder radius, R, cm	Acceleration, a, cm/sec^2	Bond number, Bo	Bubble velocity, V_o, cm/sec	Froude number, Fr
Trichlorotrifluoroethane	11.78	1.42	10.0	1.7	0.66	0.17
		2.22	10.1	4.2	1.67	.35
		2.22	10.1	4.2	1.80	.38
		1.27	36.3	5.0	2.61	.39
		2.76	10.0	6.5	2.08	.40
		2.97	10.0	7.5	2.24	.41
		2.03	36.3	12.7	3.82	.45
		4.44	9.9	16.7	3.38	.51
		4.44	19.9	33.3	4.62	.49
		4.44	39.3	65.8	6.49	.49
Anhydrous ethanol	28.25	0.79	83.3	1.8	0.87	0.11
		2.61	9.8	2.4	1.38	.27
		4.44	9.9	6.9	3.09	.47

required for the liquid-vapor interface to reach its zero-gravity configuration after entering a weightless environment is proportional to the three-halves power of the cylinder radius (ref. 13). In order to minimize the perturbation due to formation in the limited test time available, the radii of the cylinders had to be kept below 4.5 centimeters. Furthermore, practical limits to the size of spacer additions to the drag shield placed an upper limit on the acceleration level attainable consistent with a reasonable time to observe steady-state flow. The cylinder radius and acceleration limitations then restricted attainable Bond numbers to values of less than 100.

Vapor penetration rate. - Despite these practical limitations, satisfactory data in the low-acceleration regime were obtained. The latter stages of the photographic series in figure 5 clearly reveal the mode of liquid flow from the initially highly curved interface configuration. The liquid-vapor interface profile assumes the form predicted by the inviscid potential theory of Taylor with the base of the interface being spheroidal and the film thickness tapering toward the leading edge. The vapor penetration was symmetric to the axis of the cylinder in all instances, but occasionally the leading edge did not progress evenly (fig. 5(h), right cylinder). The latter effect was due to either a slight misalinement of the major axis of the cylinder with the thrust axis or an error in locating the center-of-mass axis of the package. The observed symmetry of the leading edge was extremely sensitive to even small package unbalances.

The measured vapor penetration, or ullage velocities V_o, and the pertinent system parameters in this low acceleration study are presented in table II (p. 11). The ullage velocities are shown as a function of the system parameters in figure 7 (p. 12), where the Froude-Bond number relations are identically employed to the normal-gravity experiments. The curve in figure 7 is that of equation (5), and the data points are seen to describe satisfactorily the empirical correlation represented by the equation. With the exception of the transition region of flow, the ullage velocities were observed to be constant,
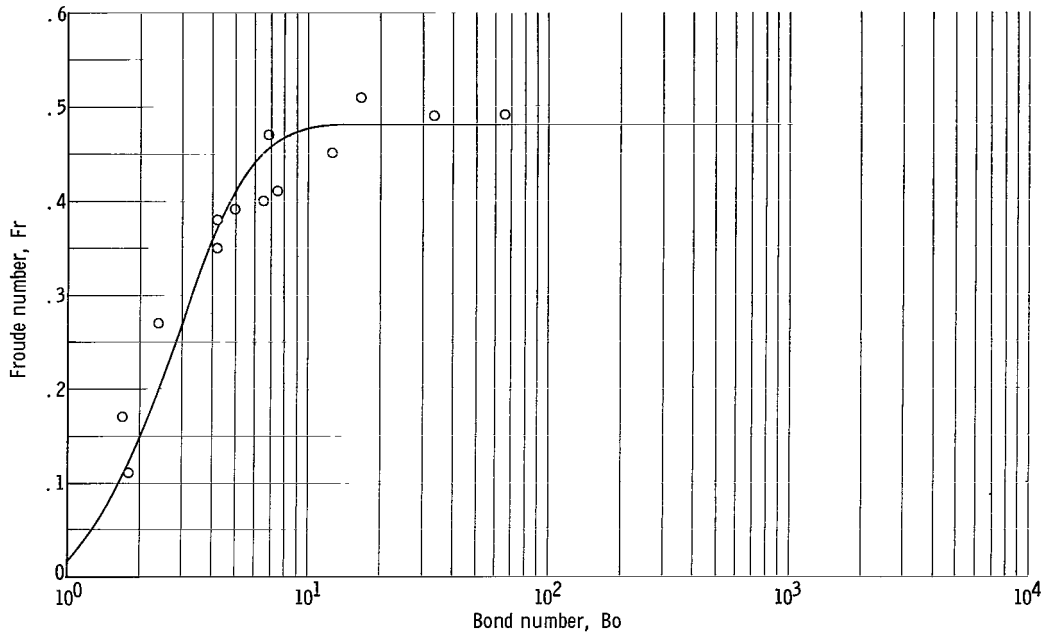
Figure 7. - Bubble velocity as function of bond number for drop-tower data. System acceleration, 0.01 to 0.08g.

as is typically shown in figures 6(a) and (b). In the larger diameter cylinders some oscillation of the ullage displacement was noted, due to either the perturbation of the formation period or more likely to the response characteristics of the pressure regulator in the thrust system of the experiment package. The oscillation, however, appeared to be highly damped, and the deviation in the steady-state flow region was so small that the average penetration was linear in time and the ullage velocity could be effectively regarded as constant. It is further noted that the velocity was constant and independent of the initial percentage of liquid filling even to the point of contact of the vapor with the flat base of the cylinder.

Leading-edge displacement. - It is apparent from both the photographs in figure 5 and the curves in figure 6 of the representative run that the displacement of the leading edge is not linear. The result is consistent with theory: if the profiles of the interfaces in response to both inertial and gravitational body-force accelerations are identical, the continuity equations demand that the leading edge accelerate, which is a necessary converse of Taylor's argument (ref. 8). The fact that the leading-edge displacement is parabolic in time is evidenced by the satisfactory curve fit typically represented in figure 6. An analysis of the leading-edge displacement characteristics led to the following equation:

$$a_L = \frac{3.8 \, V_o^2}{R}, \quad Bo > 1.7 \qquad (7)$$

where a_L is the magnitude of the leading-edge acceleration, and V_o is the ullage velocity given by equation (5). The empirical correlation of equation (7) was based on the actual ullage velocity as observed in each run and is
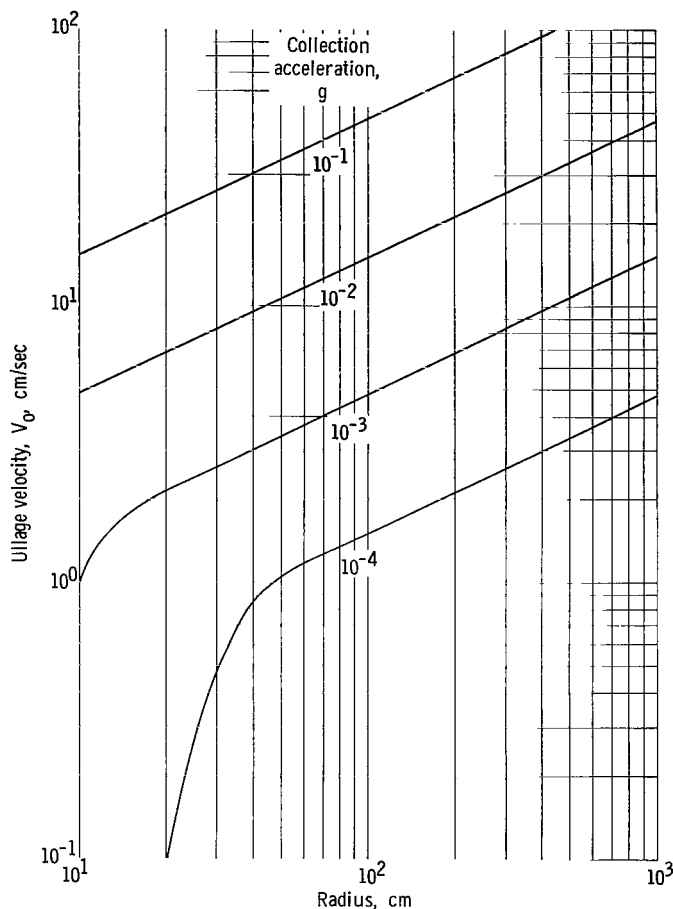
12

Figure 8. - Ullage velocity as function of radius. Specific surface tension, 28.25 centimeters cubed per second squared.

accurate to within 10 percent; the accuracy increases with increasing Bond numbers.

Substituting for V_o^2 yields

$$a_L = 0.87\, a \left[1 - \left(\frac{0.84}{Bo} \right)^{\frac{Bo}{4.7}} \right]^2$$

$$\text{for} \quad Bo > 1.7 \qquad (8)$$

For $Bo > 12$,

$$a_L = 0.87\, a \qquad (9)$$

which indicates a slight departure from the ideal situation. The validity of equation (7) and those that follow are restricted to distances comparable to two times the diameter of the cylinder, approximately the maximum distance obtainable in the present experiment. This restriction is, however, compatible with the current design of space-vehicle propellant tanks with fineness ratios of 2. The motion of the leading edge is undoubtedly viscosity dependent and, in the limited test time available, the tenuity of the conclusion that the leading edge would continue to accelerate in time is apparent. The existence of a terminal velocity is here neither disproved nor substantiated.

APPLICATION

As a result of these investigations, the ullage velocity under an imposed collection acceleration in real vehicle propellant tanks can be predicted. In figure 8 a parametric plot is presented of the ullage velocity against tank radius for one liquid that is representative of many propellants. The curve was obtained from equation (5) by extending the relation to tank radii that are currently under consideration for space vehicles. It can be seen from figure 8 that, for space vehicles having tank radii of the order of 5 feet (152.4 cm), a typically imposed collection acceleration of 10^{-2} g will result in an ullage velocity of slightly greater than 18 centimeters per second. Hence, if the percentage of residual propellant in a given tank geometry is known, an estimate can be made of the time required for the ullage to move from the assumed worst configuration at the pump portion to the vent portion of the tank.

13

Quite obviously, an idealized situation has been presented; for example, the ullage velocity correlation has been given for an unbaffled cylindrical geometry (i.e., no liquid level probes, surface tension baffles, etc.), where it has been tacitly assumed that the ullage velocity remains constant throughout the collection mode (i.e., no effect of tank extremities). The former aspect of the effect of geometry would be expected to alter the given velocity correlations, and in the presence of various internal tank hardware could even alter the regular symmetric mode of propellant flow. The latter aspect of the possible effects of tank extremities may reduce the velocity, although such a reduction has yet to be experimentally verified. As was previously stated, no observable effect on the ullage velocity due to the flat bottom of right circular cylinders had been noted in the low-acceleration investigation. While the significance of these two aspects is not to be minimized, the net adverse effect would be a reduction in the ullage velocity. Hence, figure 8 or equation (5) represents a reasonable estimate of the ullage velocity under the given collection acceleration even when the geometry is less than ideal.

While the ullage is moving at a constant rate toward the vent portion of the tank, the leading edge of the interface is accelerating toward the pump inlet portion of the tank with a magnitude given by equation (7). If the percentage of residual propellant is small, the instantaneous leading-edge velocity may become so large that "geysering" becomes a definite possibility when the liquid meets at the bottom of the tank. Hence, time estimates for complete propellant reorientation cannot be inferred only from ullage displacement considerations.

SUMMARY OF RESULTS

An experimental investigation of the velocity of the liquid-vapor interface in a cylindrical geometry was conducted in various acceleration fields ranging from 980 to 9.8 centimeters per second squared. The conditions prior to the application of the imposed acceleration resulted in an initially highly curved liquid-vapor interface. Under the stipulation that inertia flow may be assumed (i.e., small viscous forces in comparison with acceleration and surface tension forces), that the acceleration field is applied parallel to the longitudinal axis of the cylinder and positively directed from the vapor to the liquid phase, and that the solid-liquid-vapor system possesses a 0° contact angle, the investigation yielded the following results:

1. The liquid-vapor interface profile assumes the form predicted by the inviscid potential theory of Taylor.

2. The rate at which the vapor phase penetrates the liquid phase is constant and the ullage velocity may be obtained from the following empirical relation which includes Bond numbers approaching 1:

$$V_o = 0.48(aR)^{1/2}\left[1 - \left(\frac{0.84}{Bo}\right)^{Bo/4.7}\right]$$

14

where

V_O ullage velocity

a   system acceleration

R   cylinder radius

Bo   Bond number

3. The leading edge of the liquid-vapor interface is accelerating over linear distances comparable to fineness ratios of 2. The magnitude of the leading edge acceleration may be estimated from the following empirical relation:

$$a_L = \frac{3.8 \, V_O^2}{R}, \; Bo > 1.7$$

where a_L is the leading-edge acceleration and V_O is the calculated ullage velocity.

Lewis Research Center,
    National Aeronautics and Space Administration,
        Cleveland, Ohio, June 11, 1965.

APPENDIX - APPARATUS AND PROCEDURE FOR LOW-ACCELERATION INVESTIGATION

Test Facility

The experimental investigation was conducted in the Lewis Research Center Drop Tower (fig. 9), which provides a usable drop distance of 85 feet, or 2.3 seconds of unguided free fall. In this facility, air drag on the experiment package is kept below 10^{-5} g by allowing the package to fall inside a protective drag shield. The drag shield is designed with a high ratio of weight to frontal area and a low drag coefficient to minimize deviation from true free fall. The relative position of the experiment package with respect to the drag shield during a test drop is presented in figure 10. The experiment package and the drag shield fall simultaneously, yet are completely independent of each other during the drop. The accelerations imposed on the experiment package necessitated the addition of spacers to the drag shield to compensate for the added relative distance the package travels.

Figure 9. - 2.3-Second drop-tower facility.

(a) Position prior to test drop.

(b) Free fall (formation of zero-gravity configuration).

(c) Application of low-acceleration field.
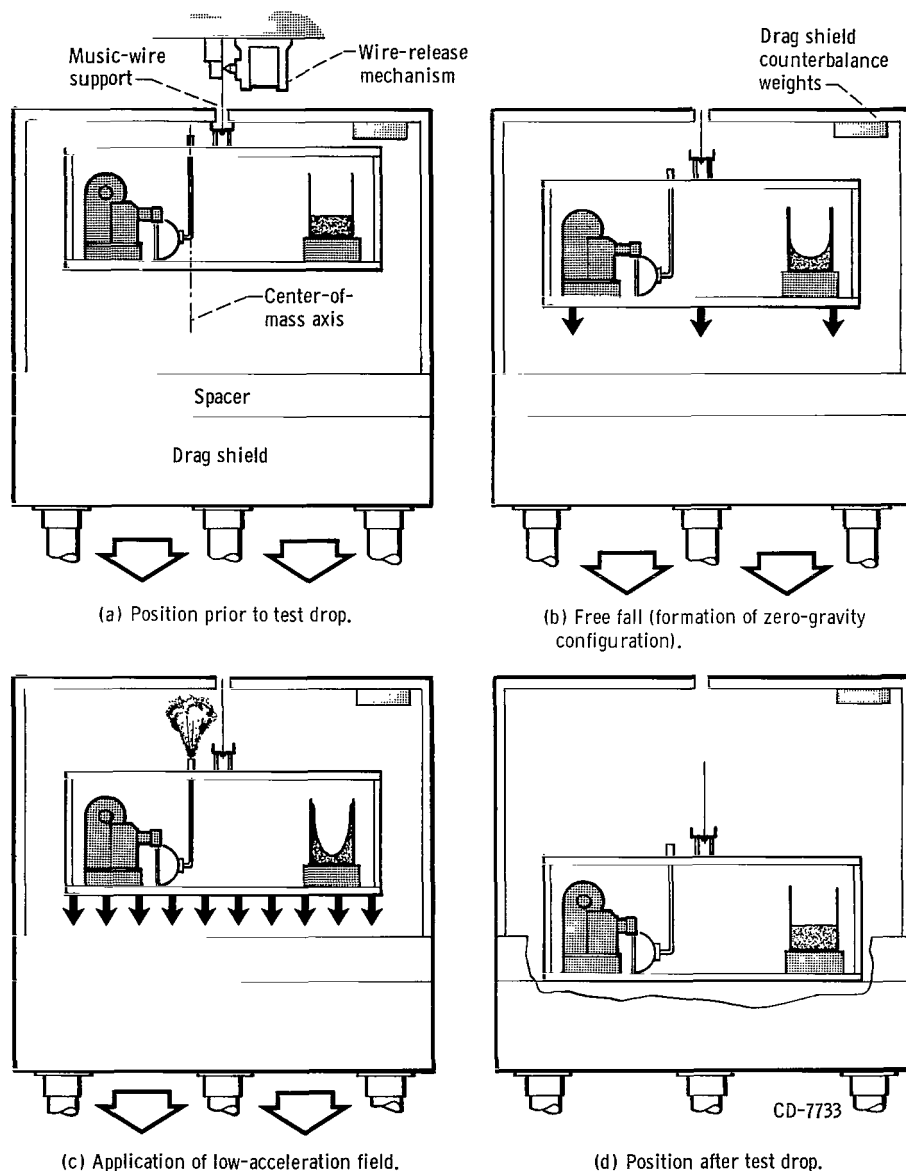
(d) Position after test drop.

Figure 10. - Schematic drawing showing sequential position of experiment package and drag shield before, during, and after test drop.

The experiment package (fig. 11) is a self-contained unit equipped to recover photographic data. Borosilicate glass cylinders containing the test liquid are suitably mounted in a box having a dull white interior and are indirectly illuminated to allow a 16-millimeter high-speed motion-picture camera to photograph the liquid behavior during the drop. Low accelerations are imposed on the experiment by expelling compressed nitrogen gas from a thrust nozzle located on top of the package. The thrustor system consists simply of a high-pressure accumulator and a fast-response pressure regulator and solenoid valve. Power to operate the electrical hardware is obtained from nickel-cadmium

17
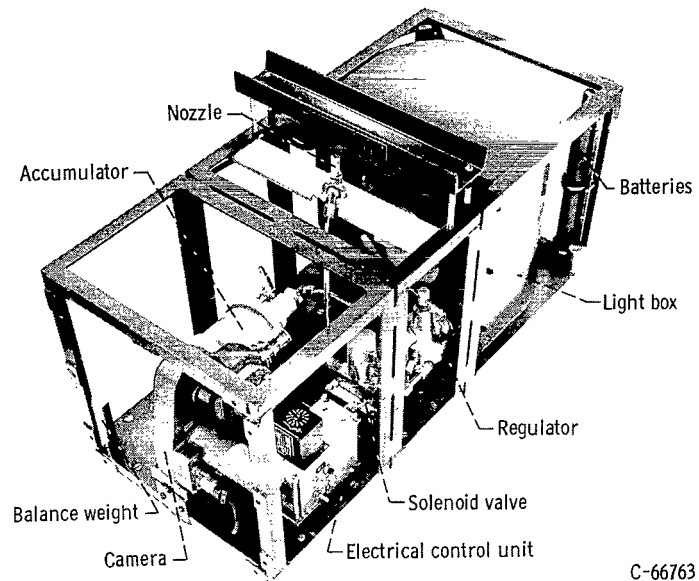
Figure 11. - Experiment package.
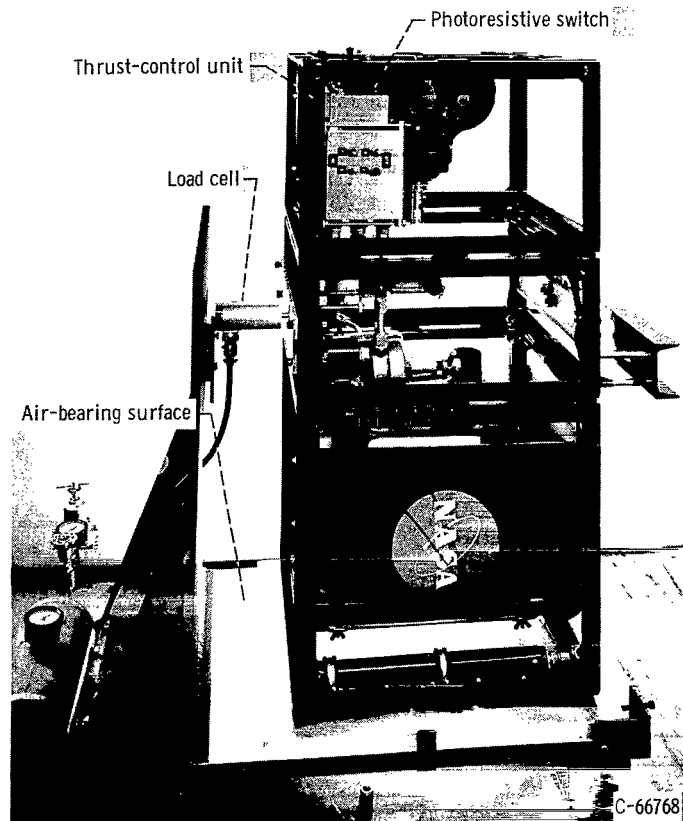
Figure 12. - Thrust calibration system.

batteries carried on the experiment package.

The liquids, their physical properties, and the parameters pertinent to this investigation are presented in table II (p. 11). The liquids possess 0° contact angles with borosilicate glass. A small quantity of dye was added to each liquid to improve photographic quality, the addition of which had no measurable effect on the liquid properties.

Operating Procedure

Prior to each test drop, the experiment package was carefully balanced to locate the center-of-mass axis on the line coincident with the thrust axis (fig. 10). The magnitude of the thrust was determined by means of the thrust calibration system shown in figure 12. The package was placed on a frictionless air bearing with the thrust incident on a strain-gage load cell mounted in line with the thrust axis. The solenoid valve was actuated by a photoresistive switch in the electrical control unit to avoid introducing a drag factor through a physical connection to the package. The actual accelerations used in this study, as determined by this calibration procedure, ranged from 83.3 to 9.8 centimeters per second squared ±4 percent (table II).

Contamination of the liquids and glass surfaces, which could alter the liquid properties and contact angle of the test liquids, was carefully avoided. A preliminary cleaning of the glassware in a detergent solution was followed by an immersion in hot chromic acid and finally by an ultrasonic cleaning in a solution of detergent and distilled water. The cylinders were then rinsed in distilled water, dried in a warm-air dryer, and filled to the desired height with the test liquid.

After the cylinders were mounted in the light box, the experiment package was placed inside the drag shield. The position of the wire support mechanism on the principal vertical axis of the package necessitated the location of the thrust axis (and hence the center of mass of the experiment package) to be off the vertical center line. The entire assembly, consisting of the drag shield and the experiment package, was counter-balanced to ensure that the assembly would not tilt when suspended from the support wire prior to the actual drop (fig. 10). Rotation of the drag shield due to the nonsymmetric mass distribution during the fall was negligible. Initiation of free fall was accomplished by pressurization of an air cylinder that forced a knife edge into the support wire and caused it to fail. The application of the acceleration was preceded by a time delay (of the order of 0.7 sec) to allow the liquid-vapor interface to form its zero-gravity configuration. This time was generally not sufficient to ensure the complete absence of oscillatory interface motion toward the unique time-independent, zero-gravity interface configuration, but represented, for the range of cylinder diameters and liquid properties used, a compromise between an adequate formation period and a sufficient time in the low-acceleration field to observe the dynamic behavior of the interface. (Further discussion of the effects of this formation period on subsequent velocity measurements is contained in the section on low-acceleration data.) Prior to deceleration in a sandbox, the package came to rest on the bottom of the drag shield, and this resulted in a usable test time of 2.15 seconds. The upper

time limits in figures 5 and 6 were due solely to camera view angle restrictions. While wide angle lenses were generally used in the investigations to make full use of the maximum test time of 2.15 seconds, selected frames from these films were usually not of sufficient quality for report reproduction.

REFERENCES

1. Otto, E. W.:   Static and Dynamic Behavior of the Liquid-Vapor Interface During Weightlessness.   Preprint 17a, A.I.Ch.E., 1965.   (Also available as NASA TM X-52016.)

2. Gluck, D. F.; and Gille, J. P.:   Fluid Mechanics of Zero G Propellant Transfer in Spacecraft Propulsion Systems.   Paper No. 862A, SAE, 1964.

3. Satterlee, H. M.; and Reynolds, W. C.:   The Dynamics of the Free Liquid Surface in Cylindrical Containers Under Strong Capillary and Weak Gravity Conditions.   Rept. No. LG-2, Stanford Univ., May 1, 1964.

4. Masica, William J.; Petrash, Donald A.; and Otto, Edward W.:   Hydrostatic Stability of the Liquid-Vapor Interface in a Gravitational Field.   NASA TN D-2267, 1964.

5. Masica, William J.; Derdul, Joseph D.; and Petrash, Donald A.:   Hydrostatic Stability of the Liquid-Vapor Interface in a Low-Acceleration Field.   NASA TN D-2444, 1964.

6. Abramson, H. Norman: Dynamic Behavior of Liquid in Moving Container.   Appl. Mech. Rev., vol. 16, no. 7, July 1963, pp. 501-506.

7. Hollister, M. P.; and Satterlee, H. M.:   Low Gravity Liquid Reorientation Study.   Rept. No. LMSC/A664570 (TXA 1592), Lockheed Missles and Space Co., May 1, 1964.

8. Davies, R. M.; and Taylor, G.:   The Mechanics of Large Bubbles Rising Through Extended Liquids and Through Liquids in Tubes.   Proc. Roy. Soc. (London), ser. A, vol. 200, no. 1062, Feb. 7, 1950, pp. 375-390.

9. Goldsmith, H. L.; and Mason, S. G.:   The Movement of Single Large Bubbles in Closed Vertical Tubes.   J. Fluid Mech., vol. 14, pt. 1, Sept. 1962, pp. 42-58.

10. Hattori, Sin-Iti: On the Motion of A Cylindrical Bubble in a Tube and Its Application to the Measurement of the Surface Tension of a Liquid.   Rept. No. 115, vol. 9, no. 7, Aeron. Res. Inst., Tokyo Imperial Univ., Jan. 1935, pp. 161-193.

11. Bretherton, F. P.:   The Motion of Long Bubbles in Tubes.   J. Fluid Mech., vol. 10, pt. 2, Mar. 1961, pp. 166-188.

12. Barr, G.:   Air-Bubble Viscometer.   Phil. Mag., vol. 1, no. 2, Feb. 1926, pp. 395-405.

13. Siegert, Clifford E.; Petrash, Donald A.; and Otto, Edward W.:   Time Response of Liquid Vapor Interface after Entering Weightlessness.   NASA TN D-2458, 1964.

"The aeronautical and space activities of the United States shall be conducted so as to contribute . . . to the expansion of human knowledge of phenomena in the atmosphere and space. The Administration shall provide for the widest practicable and appropriate dissemination of information concerning its activities and the results thereof."

—NATIONAL AERONAUTICS AND SPACE ACT OF 1958

NASA SCIENTIFIC AND TECHNICAL PUBLICATIONS

TECHNICAL REPORTS: Scientific and technical information considered important, complete, and a lasting contribution to existing knowledge.

TECHNICAL NOTES: Information less broad in scope but nevertheless of importance as a contribution to existing knowledge.

TECHNICAL MEMORANDUMS: Information receiving limited distribution because of preliminary data, security classification, or other reasons.

CONTRACTOR REPORTS: Technical information generated in connection with a NASA contract or grant and released under NASA auspices.

TECHNICAL TRANSLATIONS: Information published in a foreign language considered to merit NASA distribution in English.

TECHNICAL REPRINTS: Information derived from NASA activities and initially published in the form of journal articles.

SPECIAL PUBLICATIONS: Information derived from or of value to NASA activities but not necessarily reporting the results of individual NASA-programmed scientific efforts. Publications include conference proceedings, monographs, data compilations, handbooks, sourcebooks, and special bibliographies.

Details on the availability of these publications may be obtained from:

SCIENTIFIC AND TECHNICAL INFORMATION DIVISION

NATIONAL AERONAUTICS AND SPACE ADMINISTRATION

Washington, D.C. 20546